Tuijin Jishu/Journal of Propulsion Technology
ISSN: 1001-4055
Vol. 44 No. 5 (2023)

Mapping potential hydrocarbon sites in Upper Assam shelf using geospatial and geo-structural techniques

Ashish Aggarwal, Devesh Rajendra Umredkar, Nirlipta Nayak*
Department of Petroleum Engineering and Earth Sciences, University of Petroleum and Energy Studies, Dehradun, 248007, Uttarakhand, India

Abstract:- Remote Sensing and Spatial analysis tools are used to identify the hydrocarbon prospective zones as subsurface hydrocarbon traps are not perfectly sealed and moves in the upward direction from the reservoir to the surface in the form of traces and alter the vegetation which can be recognized through several techniques. Landsat-8 OLI and Sentinel 2A satellite images were used and spectral signatures such as Mineral Indices, Vegetation Index, Hydrothermal Alteration were analyzed to detect possible hydrocarbon sites in the study area. Mineral Indices namely clay carbonate, ferrous, and ferric indices were used to confirm and locate the hydrocarbon zones which is directly related to the detection of hydrocarbon micro seepage on the surface. Vegetation indices such as NDVI, GNDVI, SAVI, and Chlorophyll Index Green were investigated to narrow down the prospective areas, indicating chemical alteration in the soil and vegetation, giving an idea about the hydrocarbon prospective zones. Magnetic and gravity data were also collected to correlate these findings which shown anomalies in the study area and gave evidence for the prospect of hydrocarbon. Lineament extraction was performed to delineate the micro seepage zones in the study area. After combining all the data, the prospective zones of hydrocarbon and micro seepage in Upper Assam Shelf were located. Furthermore, a comparison study was conducted to identify prospective areas from analyzing both Sentinel 2A and Landsat 8 images. The results of the study demonstrated the effectiveness of remote sensing and spatial analysis tools in identifying hydrocarbon prospective areas in the region.

Keywords*: Remote Sensing, Upper Assam Shelf, Mineral Indices, Vegetation Indices, Hydrothermal Indices, Lineament.*

1. Introduction

Remote Sensing and GIS is a data acquisition method of field observation as it allows mapping of geological characteristics and petroleum aspects of a region without being in physical contact with the area being explored. They are being used as an advance technology of considerable interest for geoscientist and petroleum geologist for detecting hydrocarbon accumulation, micro seepages and macro seepages in onshore and offshore conditions (Putra et al., 2019). As they provide fast and cost-effective tools that are useful in direct and indirect method by capturing spectral reflectance of the altered minerals or surface minerals for detecting micro seepage and macro seepage (Asadzadeh & de Souza Filho, 2017).

Around 75% of the world oil basins have been detected by the micro seepages as it directly indicates the presence of hydrocarbon beneath the surface (Lammoglia & de Souza Filho, 2013). Hydrocarbon in subsurface reservoirs is trapped or sealed by some impermeable cap rocks such as evaporite and shale. However, this caps and overlying rocks and traps are not purely impermeable due to which they start moving vertically or near vertically through faults and joints to the surface due to buoyancy force which can be detected using Remote Sensing techniques (Garain et al., 2019). As the hydrocarbon reaches the surface through seepage, it causes mineral alteration in soil and geobotany shows abnormal behaviour in the vegetation such as chemical, mineralogical and colour changes in leaves, stem and trunks (Noomen et al., 2012).

In order to detect the vegetation anomalies and mineral indices, multispectral images namely Landsat 8 OLI/TIRS and Sentinel 2A MSI were used as it has visible, near infrared, shortwave infrared bands and long wave thermal bands from the electromagnetic spectrum which are used to find out the spectral reflectance of the area. Landsat 8OLI/TIRS image with 30m of resolution and Sentinel 2A MSI with 10-20 m of resolution allows to detect the changes over the planet with time including mineral alteration, vegetation anomalies, evapo-transpiration, agriculture, cloud detection, monitoring air quality, rainforest and biomass burning, volcanic activities and geological mapping (Pour & Hashim, 2015) therefore, multispectral images are used to detect the anomalies and mineral changes on the surface.

Spectral remote sensing has been successfully utilized globally and identified hydrocarbon micro seepage through band ratioing technique (Garain et al., 2019), observing mineralogical alterations such as: (a) discoloration of red soils/rocks, known as bleaching of red beds, caused by the removal of ferric iron (Fe3+) and an increase in ferrous iron (Fe2+) content. Hematite, goethite, and limonite are common ferric iron minerals found in rocks and soils; (b) the creation of clay minerals and precipitation of carbonate minerals, which occurs through the alteration of feldspars or micas and diagenetic carbonate mineral development, such as calcite or siderite, due to petroleum oxidation (Schumacher, n.d.).

Landsat 8 OLI/TIRS and Sentinel 2A- MSI satellite images are used to detect clay carbonate, ferrous content and ferric minerals as long-term micro seepages lead to prevailing of reducing environment. The following indices were used for mineral identification.

(a) Clay carbonate Indices: According to (Jiang, 2012) clay minerals are useful to determine the prospective of oil and gas. Change in oxidation and reduction environment occurred due to the presence of hydrocarbon tends to alter the mica and feldspar to clay minerals leading to an increase in clay content over micro seepage affected area(Wu et al., 2012). Similarly, carbon dioxide produced in this condition reacts with the magnesium or calcium present in the sediments and form carbonate minerals. However, the formation of carbonate minerals is directly related to the presence of magnesium or calcium minerals (Garain et al., 2021). The acids in clay minerals acts as a catalyst in the factors such as hydrocarbon generation in which there is conversion of macromolecules of hydrocarbon into low weight molecule hydrocarbon and increases the yield of hydrocarbons (Cai et al., 2022). Presence of clay minerals is important for the generation and expulsion of hydrocarbon as clay minerals and organic matters generally coexist in the source rock, the fine clay minerals are very sensitive to the changes in source rock leads to generation of hydrocarbons. During burial diagenesis, smectite is converted to illite in late-stage dehydration or replacement of kaolinite to illite and also direct precipitation of illite acts as an indicator of fluid flow or migration. Also, existence of secondary illite can indicate that water release can create the capillary action responsible for hydrocarbon migration from source rock to reservoir rock or to the surface(Asadzadeh & de Souza Filho, 2017),(Jiang, 2012). Illite as clay mineral can acts as interesting indicator for hydrocarbon as it can provide as isotope dating constrain basin heating event and precipitation in the pores of reservoir rock leading to fluid flow.

(b) Ferrous and Ferric Indices: The study area contains red and alluvial soil having higher amount of ferric minerals which get reduced to ferrous iron minerals as the reducing condition is prevailed due to the presence of hydrocarbon causing pH difference of the surrounding geology causing mineral alteration. Therefore, bleaching of iron includes reduction in ferric content and abundance of ferrous content (Garain et al., 2021). The common ferric minerals altered due to hydrocarbon micro seepage include rocks types namely hematite and goethite and get converted to ferrous mineral and form magnetite, siderite and pyrite.

The use of remote sensing data enables the monitoring of vegetation structure and condition over a wide area, facilitating the detection of changes in vegetation patterns. The chemical alterations caused by hydrocarbon micro seepage can damage the metabolism of plants and crops, leading to the occurrence of Geobotanic anomalies. These anomalies are characterized by variations in leaf size, thickness, pigment, photosynthesis rate, and thickness. To detect these anomalies (Ahmad et al., 2017) used NDVI to identify hydrocarbon seepage therefore multispectral images was utilized for vegetation indices such as NDVI, GNDVI, SAVI, and Chlorophyll Index Green. These indices are highly sensitive to changes in biomass and can provide quantitative measurements of vegetation anomalies caused by hydrocarbon micro seepage(Ahmad et al., 2017) (Balogun et al., 2020) (Putra et

al., 2019). Visible (VIR), Near infrared (NIR), and Short-Wave Infrared (SWIR) rays are employed by the vegetation index to identify oil-polluted areas based on spectral reflectance. Vegetation indices are created using the arithmetic combination of two or more spectral bands present in electromagnetic waves, and this information is obtained and reflected through satellite imagery(Balogun et al., 2020).

Detection of hydrocarbon migration is necessary as it indicate the location of reservoir rock present in the subsurface. Under tremendous pressure, hydrocarbon tends to seep through the zones of lineament along the faults to form seepage at the surface. The study(Enoh et al., 2021) was carried out to detect hydrocarbon micro seepage using lineaments as it is just a straight or nearly straight surficial expression of faults which is linked with the subsurface geomorphology. The lineaments can be extracted automatically using PCI Geomatica which provides surficial faults, joints of a particular area. Using lineament analysis and lineament density map one can categories the type of lineament (very low, low, Moderate, high, very high) with the fault map and can detect the high prospective micro seepage conduit zones (Enoh et al., 2021)(Mah et al., n.d.).

Geophysical data such as Gravity and Magnetic data also plays a vital role in determining the presence of hydrocarbon. Gravity anomalies are due to density changes in the subsurface rock while Magnetic anomalies are due to magnetic minerals present in the rock.

2. Study Area

The Upper Assam Shelf located at Lat-26˚ 49’ 15” N, Long-94˚ 28’ 14” E to Lat-26˚ 49’ 15” N, Long- 96˚ 1’ 15” E in the Eastern side of Assam Arakan Basin which is Categorized as Category-I basin. The Assam Arakan Basin which is situated at the Northeastern Part of India covers over and area of 1,16,000 sq.km.(Assam-Arakan Basin, n.d.). The study area (Upper Assam Shelf) covers an area of 7,409 sq Km. including the region of Naga Schuppen Belt of Assam region and major Oil and Gas field- Digboi, Naharatiya, Lakwa and Moran (Figure 1).

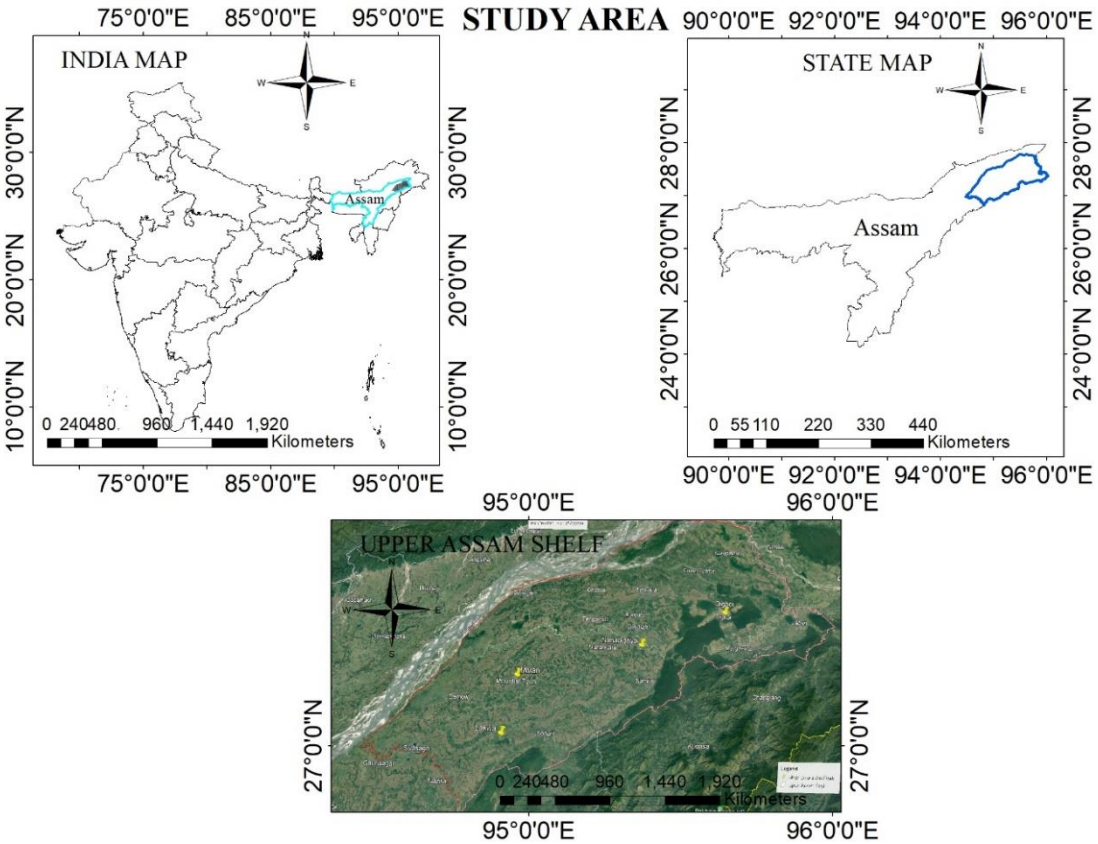

Figure 1- Study Area (Upper Assam Shelf)

3. Geology

The study area has low elevation as it is a basinal structure (Figure 2) and contains younger sheets of sedimentary rock ranging from Miocene to Plio- Pleistocene of Assam Himalayan foothills and it was deposited under fluvio-deltic environment followed by marine transgression. During the end of deposition of Tipam Sandstone, there was development of series of N-S trending compressive structures in basinal area and due to the growth of compressive structures there was deposition of Girujan Clay Formation in synclinal basin (Cachar basin). In Upper Assam there was significant milestone in oil exploration during 1953, 1956, and 1960 and discovered Naharkatiya, Moran, and Rudrasagar respectively, along that more than 100 oil and gas fields were also discovered including Kumchai, Hapjan, Lakwa, Amguri, Charali, Shalmari, Geleki, Khoraghat, Dirok, Baghjan, Jorajan (Assam-Arakan Basin, n.d.).

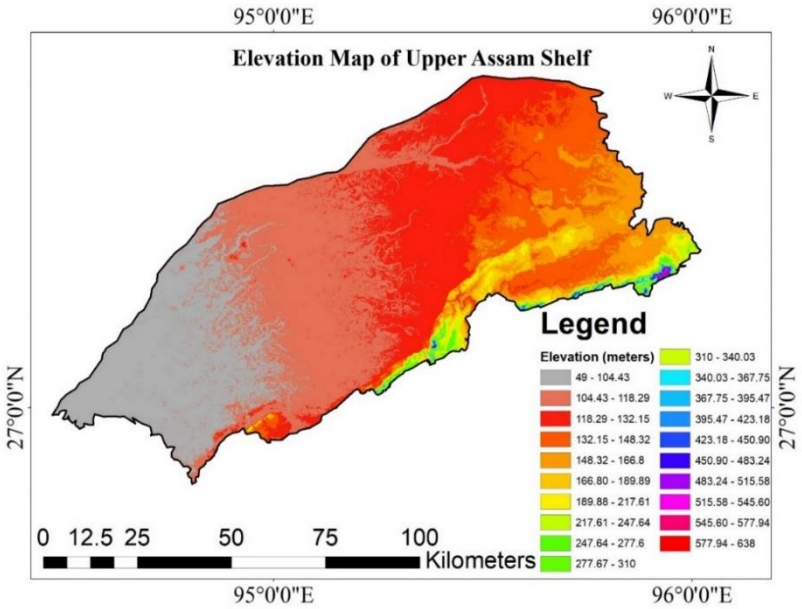

Figure 2 - Elevation Map of Study Area (Upper Assam Shelf)

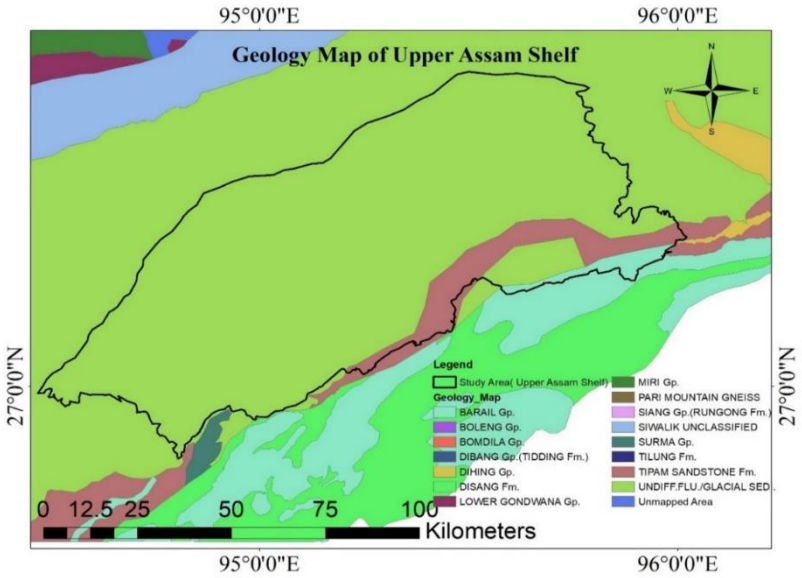

Figure 3- Geological Map of Study Area (Upper Assam Shelf)

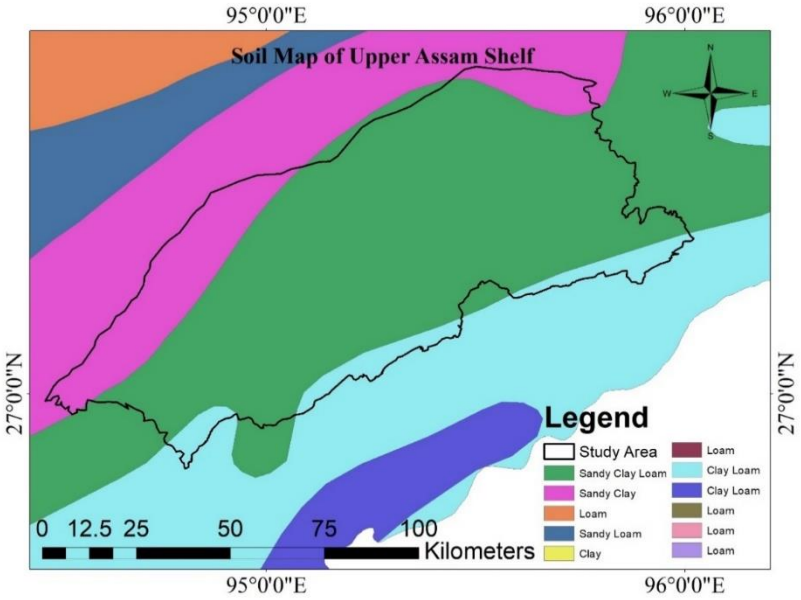

Figure 4- Soil Map of Study Area (Upper Assam Shelf)

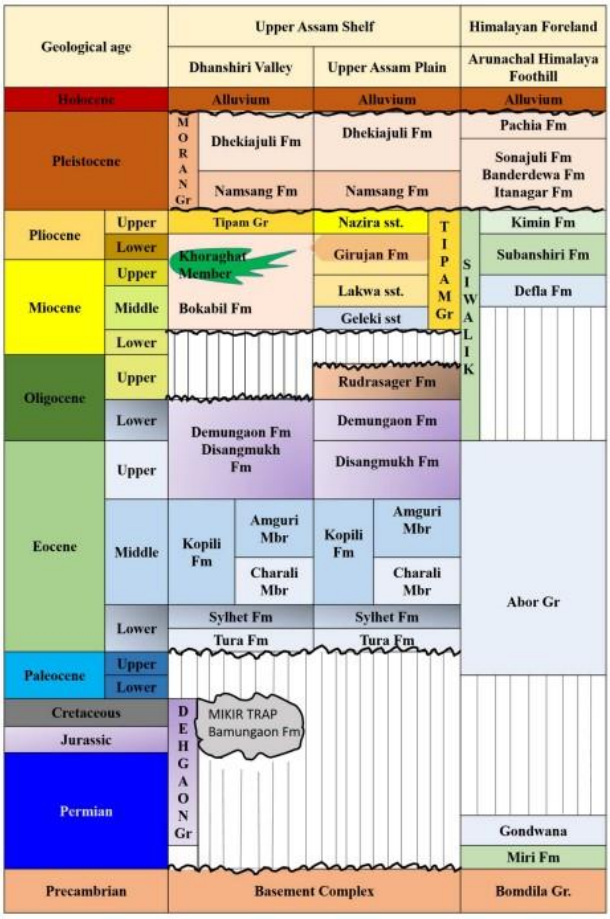

Figure 5- Stratigraphy of Assam Arakan Basin *(Boruah et al., 2022)*

In Upper Assam, Barail Group (Upper Eocene to Lower Oligocene age) and Tipam Group (Upper Miocene age) have been the primary locations for discovering Oil and Gas fields. Additionally, two major oil fields, Kharsang and Digboi, were discovered in the Naga Schuppen zone with oil reserves in Upper Miocene to Pliocene

reservoir(Enoh et al., 2021). The stratigraphy of Upper Assam can be broadly classified into Tura Formation of Eocene age, followed by Kopili fm, Disangmukh fm., Rudrasagar fm., Geleki sst., Lakwa sst., Girujan fm., Nazira sst., Namsang Fm., and Dhekiajuli fm. (Boruah et al., 2022) (Figure 5).

4. Methodology

The study involves various methods to detect the hydrocarbon zones in Upper Assam Shelf having micro seepage through the below mentioned processes (Figure 6).

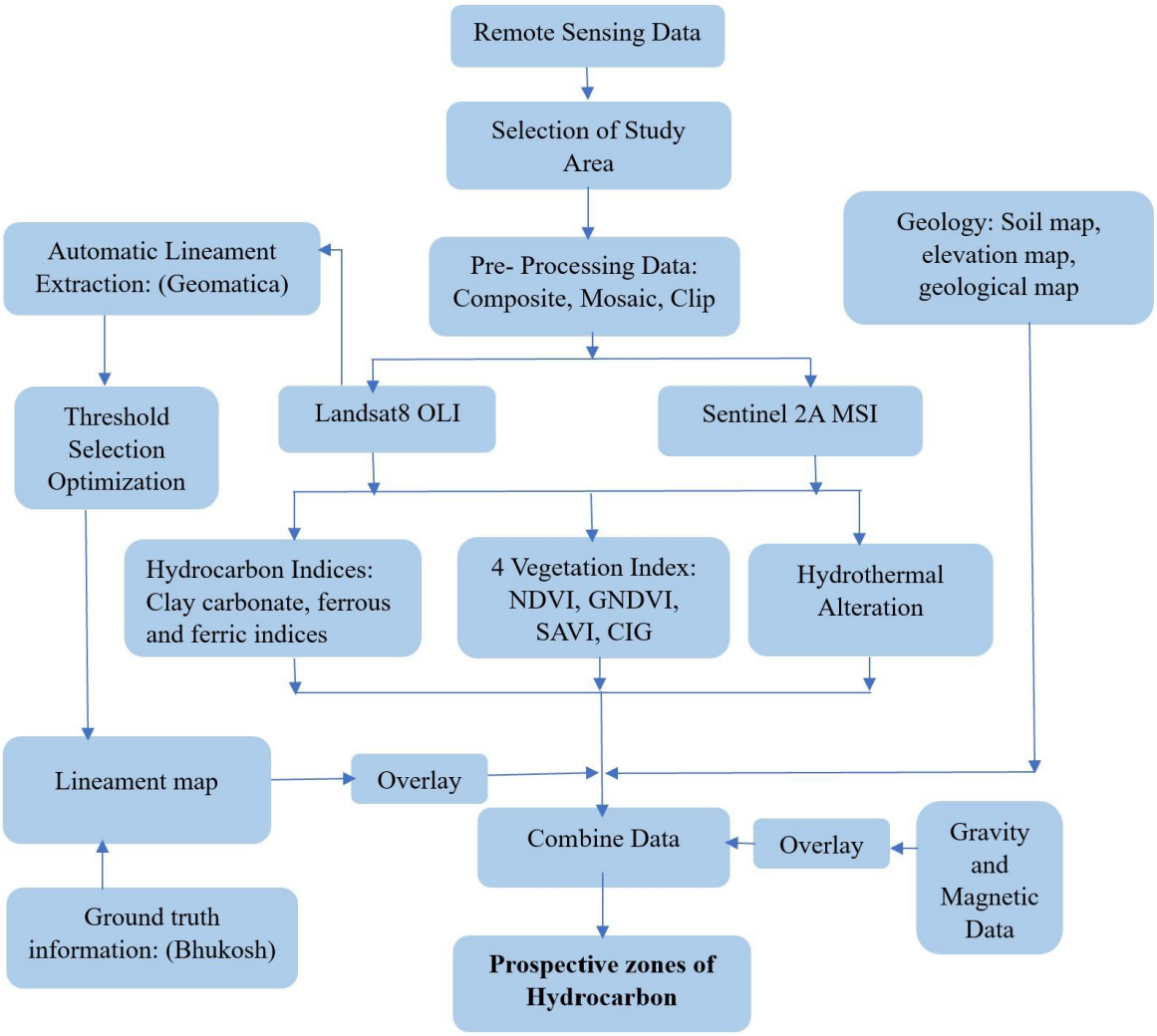

Figure 6- Flowchart of the Methodology

4.1 Data

4.1.1. Landsat 8 OLI

Landsat 8 Operational Land Imager (OLI) is a multispectral data which was downloaded through USGS data portal (https://earthexplorer.usgs.gov/) having 30m spectral resolution for 20, 29th January 2023 with cloud cover less than 5%. The raw dataset includes the following 2 files with the image projection of Universal Transverse Mercator zone 47N from WGS 1984 datum.

Table 1. Landsat 8-9 OLI-TIRS Data used

S No.	Date of Acquisition	File Name
1.	13/01/2023-20/01/2023	LC08_L2SP_135041_20230120_20230131_02_T1
2.	29/01/2023-27/02/2023	LC08_L2SP_134041_20230129_20230227_02_T1

This data contains 9 bands out of which 4 VIR (visible rays), 1 NIR (near infrared), 2 SWIR (Short wave infrared) and 2 TIR (thermal Infrared) are useful for the analysis as mentioned in Table2.

Table 2. Specifications of Landsat 8-9 OLI-TIRS

Band Names	Description	Wavelength	Resolution
Band 01	Ultra Blue	443 nm	30 m
Band 02	Blue	482 nm	30 m
Band 03	Green	561.5 nm	30 m
Band 04	Red	654.5 nm	30 m
Band 05	Near Infrared	865 nm	30 m
Band 06	Shortwave Infrared 1	1608.5 nm	30 m
Band 07	Shortwave Infrared 2	2200.5 nm	30 m
Band 10	Thermal Infrared 1	10895 nm	30 m
Band 11	Thermal Infrared 2	12005 nm	30

4.1.2. Sentinel 2A- MSI

Sentinel 2A Multispectral Instrument (MSI) is also a multispectral image instrument with spatial resolution of 10m, 20m, and 60m depending upon wavelength. The data was downloaded from Copernicus Open Access Hub (https://scihub.copernicus.eu/dhus/#/home). The Sentinel 2A data was of 5,8 January 2023 with cloud cover less than 5%. The raw data includes the following 5 files of the study area that contains 14 Bands of 20 m resolution, 7 Bands of 10 m resolution and 15 Bands of 60 m resolution out of which 12 bands of 20m resolution which was taken for study purpose. The raw dataset includes the following 5 files with the image projection of Universal Transverse Mercator zone 47N from WGS 1984 datum (Table 3).

Table 3. Sentinel 2A Data details

S.No.	Date of acquisition	File name
1.	05/01/2023	S2A_MSIL2A_20230105T041141_N0509_R047_T46RGR_20230105T074802
2.	08/01/2023	S2A_MSIL2A_20230108T042151_N0509_R090_T46RFQ_20230108T073452
3.	08/01/2023	S2A_MSIL2A_20230108T042151_N0509_R090_T46RFR_20230108T073452
4.	08/01/2023	S2A_MSIL2A_20230108T042151_N0509_R090_T46RGQ_20230108T073452
5.	08/01/2023	S2A_MSIL2A_20230108T042151_N0509_R090_T46RGR_20230108T073452

4.2 Data Pre-Processing

The pre-processing of the data performed in ArcGIS environment where the raw data of Landsat 8 and Sentinel 2A were extracted and composite was made of all the bands for both the satellite images. The composite data was processed by mosaicking to convert it into single image and clipped with the study area. The clipped image of Landsat 8 and Sentinel 2A study area are given below (Figure 7 and 8).

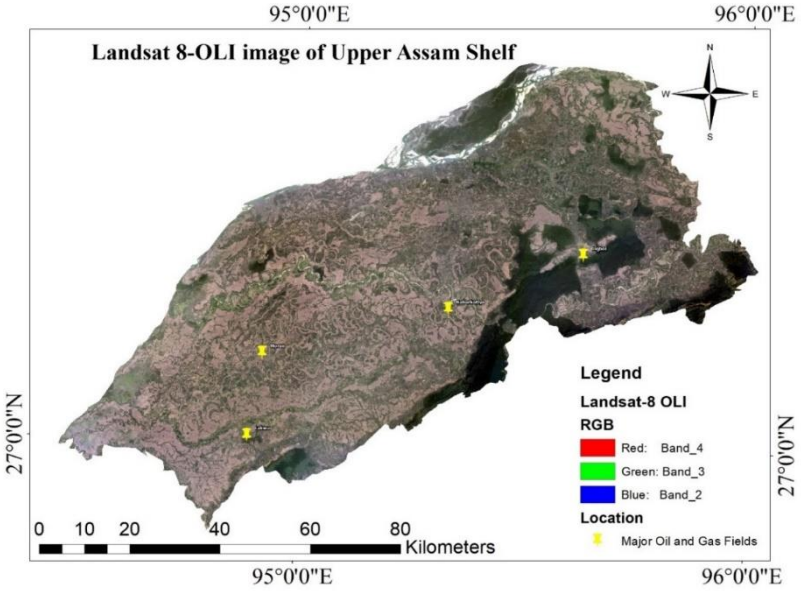

Figure 7- Landsat 8- OLI Image of Upper Assam Shelf

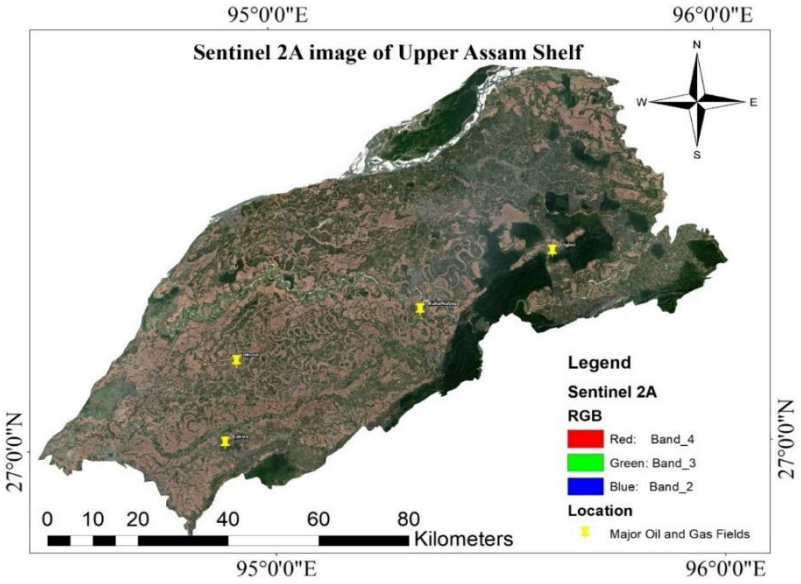

Figure 8- Sentinel 2A image of Upper Assam Shelf

4.3. Mineral Indices (Band Ratio)

Mineral indices are necessary as it directly co-relates with the hydrocarbon micro seepage in the area. Contact between hydrocarbon and soil leads to mineral alteration such as precipitation of clay carbonates, bleaching of red beds or soil, decrease in ferric content and increase in ferrous content (Garain et al., 2019, Noomen et al., 2012, Schumacher, n.d.) (Figure 9). Band ratio is been widely applied for mineral exploration to detect anomalies. Generally, mineral indices include ratio of 2 bands and not on individual bands (El-Desoky et al., 2022).

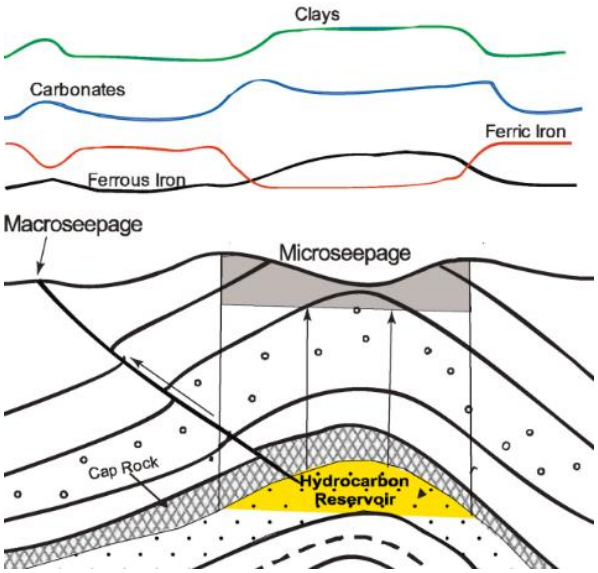

Figure 9- Relation of Mineral Indices with hydrocarbon micro seepage *(Garain et al., 2021)*

These mineral indices were used to detect the mineral alteration which are as follows:

4.3.1. Clay Carbonate indices:

Changes in the environmental condition due to presence of hydrocarbon leads to alter feldspar and mica into clay minerals leading to increase in the clay content likewise in this prevailing condition carbon dioxide is produced which reacts with calcium and magnesium to form carbonate minerals (Cai et al., 2022) (Garain et al., 2021) (Jiang, 2012). Therefore, Clay carbonate indices can be measure by using ratio of 2 SWIR bands i.e., ratio of SWIR1/ SWIR2 as the hydrous mineral such as clay and alunite absorb radiation in 2000-2300 nm portion of spectrum because it is the ratio of reflected radiation energy to the incident radiation energy (Alasta, 2011) (Gasmi et al., 2022). According to the given ratio for Landsat 8 and Sentinel 2A, Clay carbonate indices will be SWIR 1 / SWIR 2 = Band6(1608.5 nm) / Band7(2200.5 nm) and SWIR 1/ SWIR 2 = Band 11(1613.7nm)/ Band 12 (2205.5nm) respectively.

4.3.2. Ferric Indices:

As the study area has red and alluvial soil having higher amount of ferric minerals and can get converted to ferrous minerals due to prevailing reduction environment created to due to the pH difference (Garain et al., 2021). Therefore, ferrous minerals can be measure by using the ratio of SWIR band with NIR band i.e., ratio of SWIR 1/ NIR (Gasmi et al., 2022) (Mahboob et al., 2019). Ferrous mineral ratio is geological index to find the rock features having iron bearing using this band combinations. Ferric indices use this ratio because these minerals absorb radiation in 1600-850 nm (Gasmi et al., 2022) (Mahboob et al., 2019) therefore, according to the given ratio Landsat 8 and Sentinel 2A, ferric indices will be SWIR1/ NIR = Band6(1608.5nm)/ Band5(865nm) and SWIR 1/ NIR = Band 11(1613.7nm)/ Band8(864.7nm) respectively.

4.3.3. Iron Oxide:

It is the ratio of red band with blue band wavelengths because the presence of limonitic iron oxide and limonitic bearing phyllosilicates alteration causes absorption in the blue band and reflection in red band which makes the image into bright colour of iron alteration. As iron oxide show good mineral reflection in red band and absorption in blue band (670-480 nm) therefore, ratios for both Landsat 8 and Sentinel 2A of red band/ blue band will be Band 4(670 nm)/ Band 2(480nm) (Mahboob et al., 2019).

Table 5- Mineral indices for Landsat 8 and Sentinel 2A

Mineral Indices	Band Ratio	Wavelength	Landsat-8	Sentinel 2A
Clay Carbonate minerals	SWIR 1/ SWIR 2	2000- 2300nm	Band6/ Band7	Band11/ Band12
Ferrous minerals	SWIR 1/ NIR	1600- 850nm	Band6/ Band5	Band11/ Band8
Iron Oxide	Red/ Blue	670- 480nm	Band4/ Band2	Band4 / Band2

4.4 Vegetatation Anomalies

To detect the hydrocarbon micro seepage, it is necessary to observe the vegetation anomalies as it causes changes in vegetation, damage of crop and its metabolism, changes in leaf size, thickness, pigment and rate of photosynthesis. This can be detected using multispectral image namely Landsat8 and Sentinel 2A using NDVI, GNDVI, SAVI and Chlorophyll Index Green. This vegetation index is useful to identify the anomalies caused by hydrocarbon on the crops and can be determine using different vegetation state namely high greenness- not affect by hydrocarbons, low greenness- highly affected by hydrocarbons and no greenness- no vegetation (Putra et al., 2019, Kovalev & Tokareva, n.d.). Therefore, vegetation indices can be measured by the arithmetic combination of 2 or more spectral bands present in the electromagnetic waves (Balogun et al., 2020). For each vegetation there are different band ratio combination which reflects the vegetation state of the study area which were calculated in ArcGIS environment. Figure 10 below shows the reflectance curves for vegetation in different spectral regions.

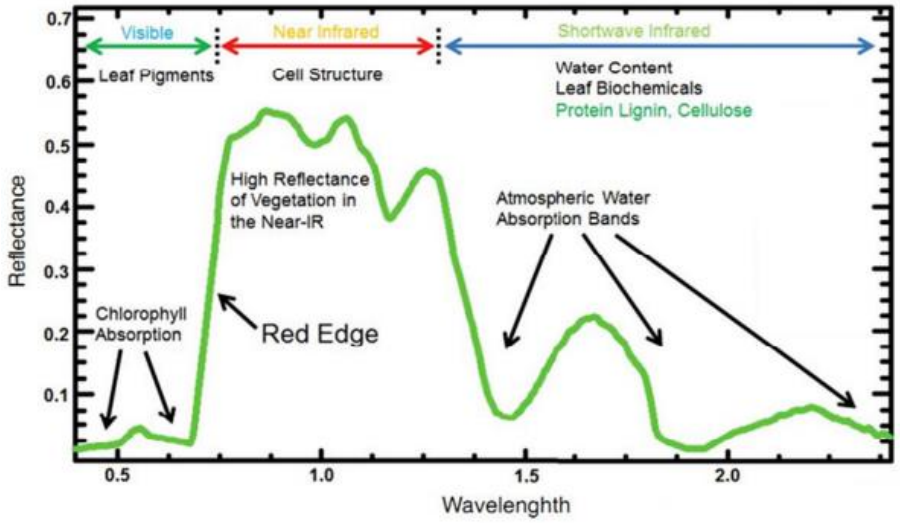

Figure 10- Spectral wavelength Vs Reflectance curve for vegetation (https://core.ac.uk/download/pdf/234664812.pdf)

- **NDVI, GNDVI, SAVI, CIG**

NDVI (Normalized Difference Vegetation Index), GNDVI (Green Normalized Difference Vegetation Index), SAVI (Soil Adjusted Vegetation Index) and CIG (Chlorophyll Index Green) are used to monitor and identify the vegetation changes and its health as hydrocarbon change bring chemical changes in the vegetation through damage of crops and its metabolism, photosynthesis pigments which will reduce their colour and the amount of chlorophyll detected in their leave (Adamu et al., 2015) (Balogun et al., 2020) (Kovalev & Tokareva, n.d.) (Putra et al., 2019). NDVI can be calculated from visible and near infrared spectrum light which is reflected by the vegetation. The healthy vegetation generally absorbs all the visible light incoming into them and reflects high amount of near-infrared lights whereas unhealthy or sparse vegetation reflects less near infrared light and reflects more visible lights (Ahmad et al., 2017). Therefore, NDVI formula is the ratio of NIR band and RED band i.e., NDVI = (NIR-RED)/ (NIR+ RED) (Balogun et al., 2020) (Kovalev & Tokareva, n.d.). GNDVI can be calculated with the green visible light and near infrared spectrum light which is reflected by the vegetation. The healthy vegetation will

absorb all the green spectra incoming and reflects all the near infrared light while unhealthy or sparse vegetation reflects green spectra and reflects less near infrared lights. Therefore, GNDVI formula is the ratio of NIR bands with Green Bands i.e., GNDVI = (NIR-GREEN)/(NIR+GREEN). Similar to NDVI, SAVI also reflects in NIR band and RED band just after applying the canopy background adjustment factor "L" which is usually 0.5. therefore, the ratio is given as {(NIR- RED)/ (NIR+ RED+L)} *(1+L) (Balogun et al., 2020). CIG is used to measure the chlorophyll content of the leaf of the plants based on the band ratios which shows reflectivity in NIR and GREEN as it directly reflects the vegetation state at the wavelength of 830-560nm of the particular area. Hence the ratio is given as CIG = NIR/ Green – 1.

Table 6- Vegetation indices for Landsat 8 and Sentinel 2A

Vegetation Index	**Band Ratio**	**Landsat-8**	**Sentinel 2A**
NDVI	(NIR- RED) / (NIR+ RED)	(Band5 - Band4) / (Band5+ Band4)	(Band8- Band4) / (Band8+ Band4)
GNDVI	(NIR - GREEN) / (NIR+ GREEN)	(Band5 - Band3) / (Band5+ Band3)	(Band8- Band3) / (Band8+ Band3)
SAVI	{(NIR-RED)/(NIR+RED+L)} *(1+L)	{(Band5 - Band4) / (Band5+Band4+L)} *(1+L)	{(Band8- Band4) / (Band8+Band4+L)} *(1+L)
CIG	(NIR) / (GREEN) - 1	(Band5) / (Band3) -1	(Band8) / (Band 3) -1

4.5 Hydrothermal Alteration

Addition to Vegetation indices and mineral indices hydrothermal altered zones was identified using multispectral image Landsat8 to detect the hydrothermally altered minerals namely clay(hydroxide), carbonate, ferrous and ferric minerals using ENVI Classic 5.3. Hydrothermal alteration is caused due invasion of hot fluids in the host rock and interact with it resulting to change in chemical composition and as the fluids cools, they get precipitate and also tend to change the lithology of the host rock by hydrothermal alteration (Imbroane et al., 2007). Several RGB combinations and Band ratios was created for Landsat 8 images based on the laboratory spectra. Different band combinations show different hydrothermally altered minerals. In order to find the particular mineral alteration band ratio technique is used in which values of one band is divided by the values of another band. The main objective of the hydrothermal alteration is to determine individual minerals for a mixed image. Hydrothermal alteration for clay carbonate minerals have absorption features of 2000nm to 2400nm and reflectance of 1550nm to 1750nm(Pour & Hashim, 2015) therefore for Landsat8 it is the ratio of Band6/ Band7, Iron oxide have high reflectance between 630nm to 690nm and have high absorption between 450nm to 520nm(Pour & Hashim, 2015) therefore for Landsat8 the band ratio is Band4/ Band2, ferrous mineral have high reflectance between 1550nm to 1750nm and have high absorption between 850nm to 870 nm therefore for Landsat8 the band ratio is Band6/ Band5.

4.6 Lineaments

As lineament is the surface and subsurface expression of faults which reflect the migration path for hydrocarbon leading to micro seepage on the surface therefore it is necessary to detect the prospective zones of hydrocarbon migration to the surface (Figure 11). Lineament extraction is considered as one of the most important parameters as far as petroliferous basin are concerned (Prabaharan et al., 2013).

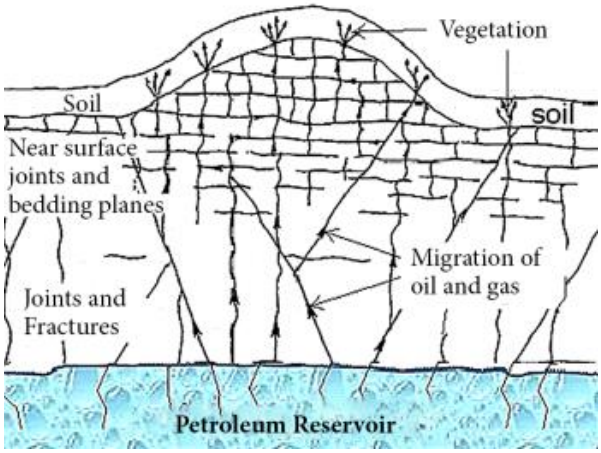

Figure 11- Relation of lineaments and hydrocarbon micro seepage *(Schumacher, n.d.)*

In the present study area surface Lineament extraction was performed (Figure 12) on the multispectral Landsat8 image using PCI Geomatica (Catalyst Professional) with optimum Threshold values mentioned below (Table 7).

Table 7- Threshold for lineament extraction

S No.	Parameter settings	Values
1	Filter Radius (Pixel)	10
2	Edge Gradient Threshold	100
3	Curve Length Threshold (Pixel)	50
4	Line Fitting Error (Pixel)	3
5	Angular Difference Threshold (Degree)	45
6	Linking Distance Threshold (Pixel)	100

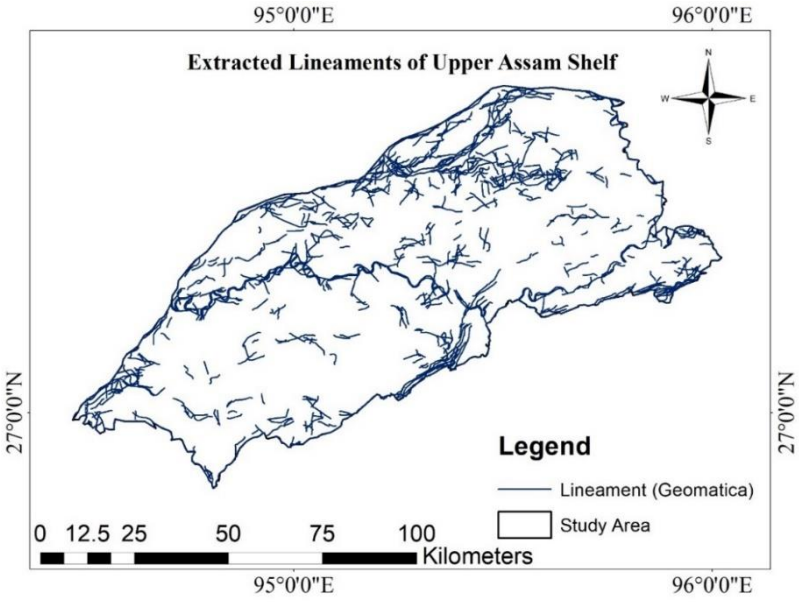

Figure 12- Extracted Lineament Map of Study Area

The extracted Lineament has co-related with the fault map from GSI Bhukosh (https://bhukosh.gsi.gov.in/Bhukosh/MapViewer.aspx) to determine the exact location of faults and fractures leading to micro seepage of hydrocarbon (Figure 13).

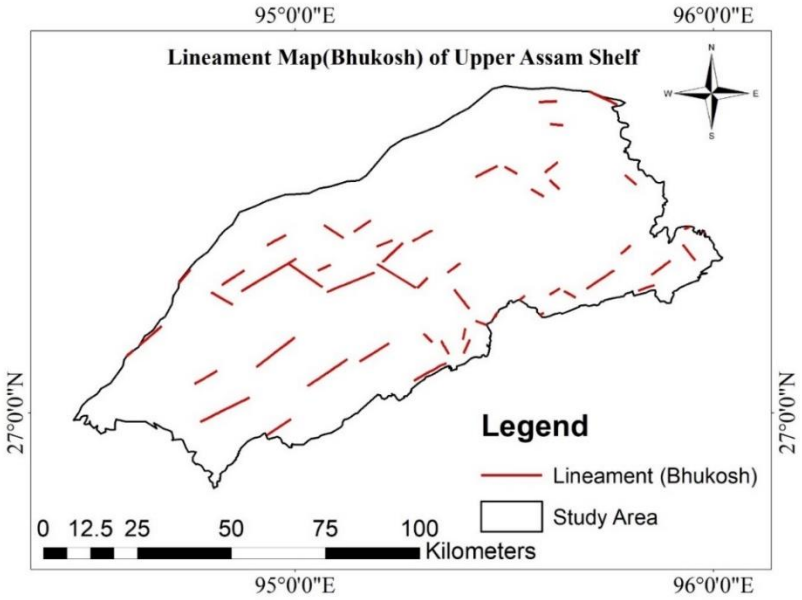

Figure 13- Lineament Map downloaded for Bhukosh

4.7 Geophysical Data (Gravity and Magnetic Data)

Geophysical data help to determine the prospective zones of reservoir rock as it shows gravity and magnetic anomalies in the particular region. The satellite gravity data was obtained from https://topex.ucsd.edu/cgi-bin/get_data.cgi website of NOAA (Garain et al., 2019) and magnetic data was obtained from https://www.ngdc.noaa.gov/geomag. Hydrocarbon micro seepage prospective zones derived by remote sensing shows low gravity, where the hydrocarbon is very high due to storage in reservoir rock (Garain et al., 2019). As earth's gravity depends upon the density of the subsurface rock and hydrocarbons are present generally in sedimentary rock namely shale and are stored in reservoir rock namely sandstone, limestone dolomite etc. having less density than igneous and metamorphic (Garain et al., 2021). Therefore, it can be interpreted as the prospective zones of hydrocarbon have low gravity. According to the result, the study area shows values ranging from -1.78 to -1.15 mGal (Figure 14) which indicates the presence of gravity anomalies and similar result was obtained from (Garain et al., 2021) Silchar area.

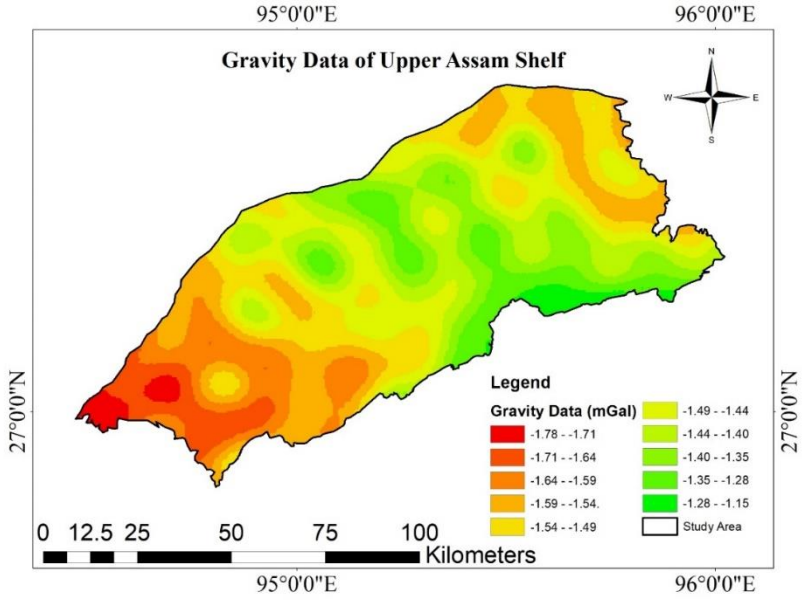

Figure 14- Gravity Data of Study Area (Upper Assam Shelf)

The magnetic data are also related to the prospective zones of hydrocarbon reservoir as several studies suggested that hydrocarbon seepage leads to form of magnetic minerals which ultimately leads to high magnetism (Garain et al., 2021). Therefore, the presence of hydrocarbon reservoir indicates high magnetic values and study area shows value ranging from 33,100 to 34,400 nT (Figure 15).

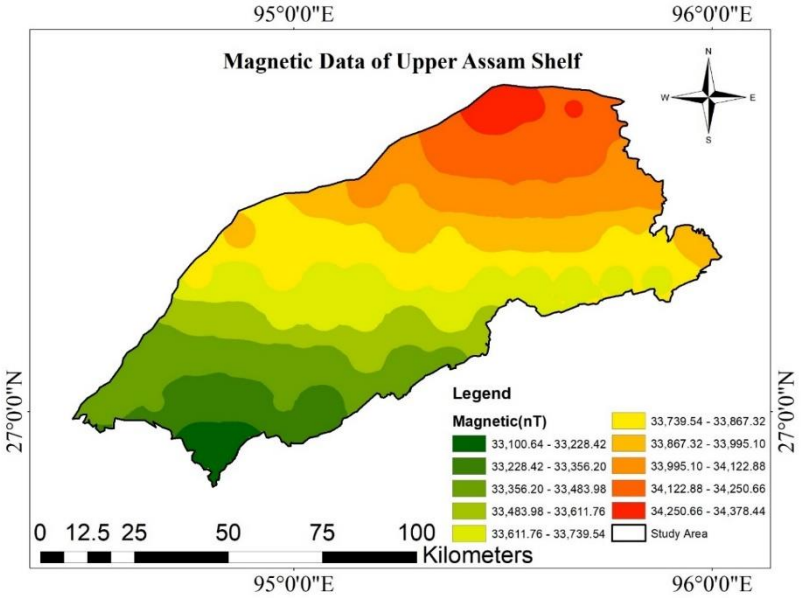

Figure 15- Magnetic Data of Study Area (Upper Assam Shelf)

High magnetism can also indicate the presence of shallow basement region but as gravity data is low which indicates that the basement is not shallow(Burazer et al., 2001) (Jiang, 2012). Both gravity and magnetic data was converted to contour map in ArcGIS and later converted to respective values.

5. Results

In order to determine the Prospective zones of Hydrocarbon in Upper Assam Shelf, two Satellite images were used namely Landsat 8-OLI and Sentinel 2A for better results as they are multispectral image which can easily detect the spectral signatures.

5.1 Mineral Indices

Mineral Indices gives direct evidence for presence of hydrocarbon on the surface therefore Clay Mineral Indices, Ferrous Mineral Indices and Iron Oxide Indices has performed in which Clay Carbonate Indices shows value of 1.42 in (Figure 16) and 2.09 in (Figure 17) as higher values in red colour for Landsat 8 and Sentinel 2 respectively. Similarly, Ferrous Indices shows value of 2.60 in (Figure 18) and 3.90 in (Figure 19) as higher values in red colour for Landsat 8 and Sentinel 2 respectively and Iron oxide shows value of 1.51 in (Figure 20) and 2.04 in (Figure 21) as higher value in red colour. Higher values indicating the mineral alteration which gave direct evidence of presence of hydrocarbon due to micro seepage as stated earlier. Therefore, common area was marked from all Mineral Indices map and found the common mineral alteration zones.

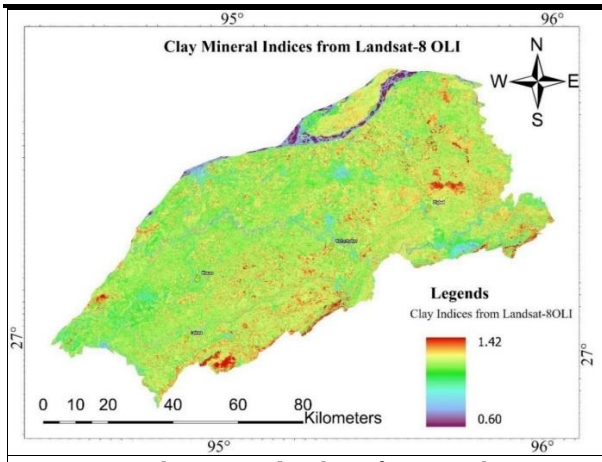

Figure 16- Clay Mineral Indices from Landsat 8-OLI image

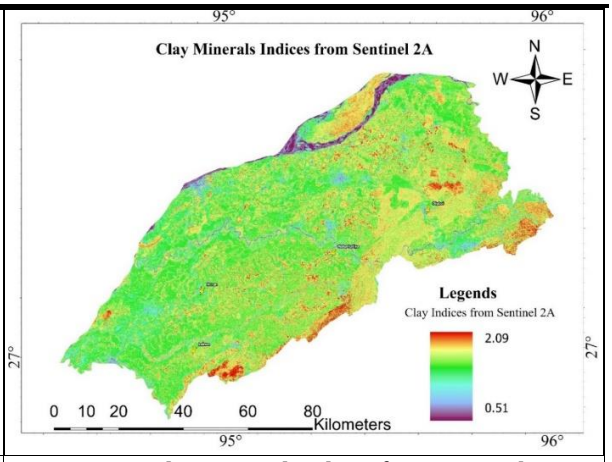

Figure 17- Clay Mineral Indices from Sentinel 2A image

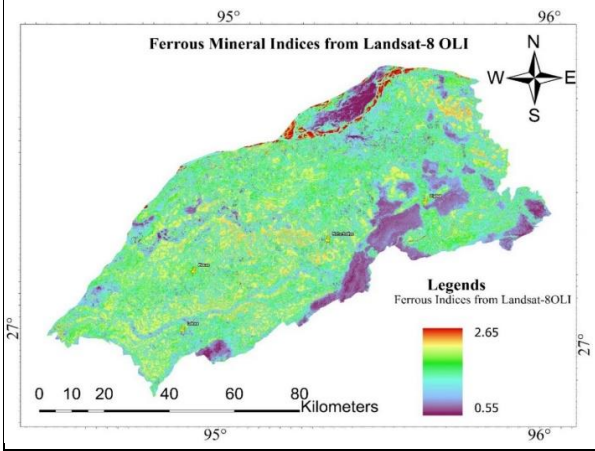

Figure 18- Ferrous Mineral Indices from Landsat 8-OLI image

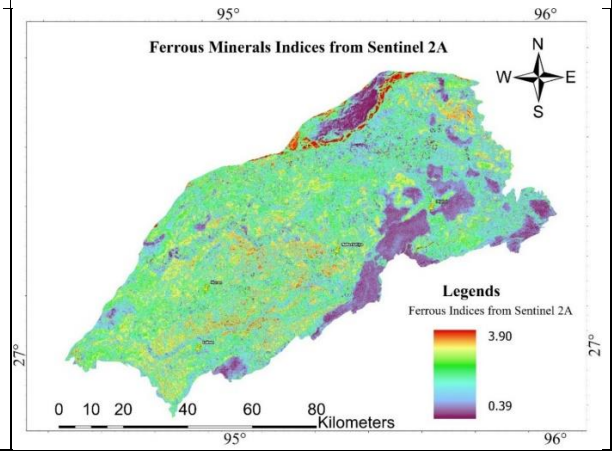

Figure 19- Ferrous Mineral Indices from Sentinel 2A image

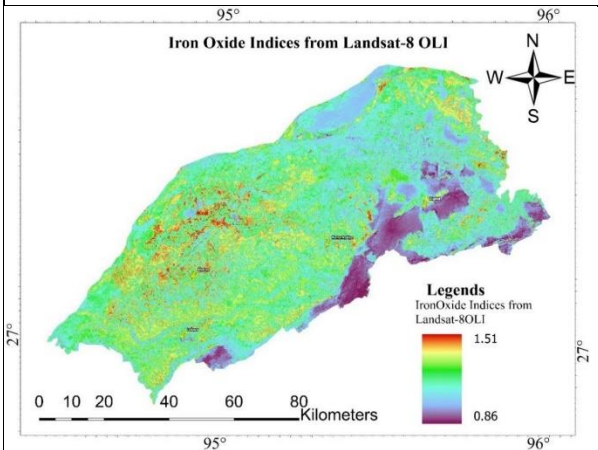

Figure 20- Iron Oxide Indices from Landsat 8-OLI image

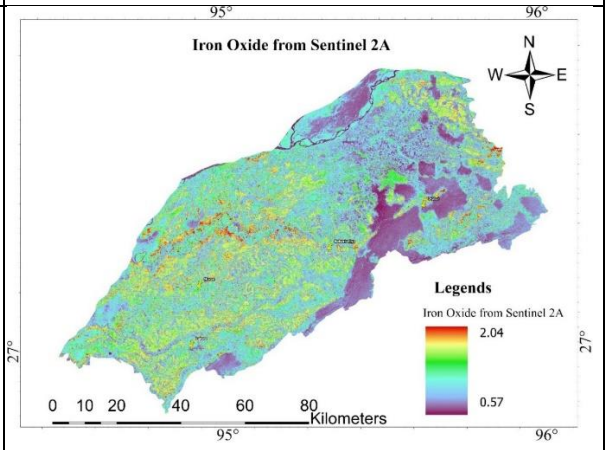

Figure 21- Iron Oxide Indices from Sentinel 2A image

5.2 Geobotanic Anomalies (Vegetation Index)

Vegetation indices were used (NDVI, GNDVI, SAVI and Chlorophyll Index Green), NDVI image of Landsat-8 and Sentinel 2A shows the value ranging from 0.44 to -0.07 in (Figure 22) and 0.71 to -0.27 in (Figure 23) respectively indicates the higher value in red colour which means that vegetation should be high but according to the researchers Landsat 8 values for NDVI the value 0.7 is for luxuriant vegetation, 0.5 for sparse vegetation, 0.025 for soil, 0 for clouds, -0.05 for snow and ice, -0.25 for water and -0.5 for man-made materials while for Sentinel 2 NDVI the values 0.9 is for luxuriant vegetation, 0.7 for sparse vegetation, 0.5 for soil (Kovalev & Tokareva, n.d.), so accordingly NDVI image with value 0.5 for Landsat 8 shows sparse vegetation in (Figure 22) and a value 0.7 for Sentinel 2 shows sparse vegetation in (Figure 23). These indices indicate vegetation anomalies due to chemical alteration. Similarly, for GNDVI (Figure 24 and 25), SAVI (Figure 26 and 27), Chlorophyll Index Green (Figure 28 and 29) shows red colour as higher values in Landsat-8 and Sentinel 2 shows sparse vegetation.

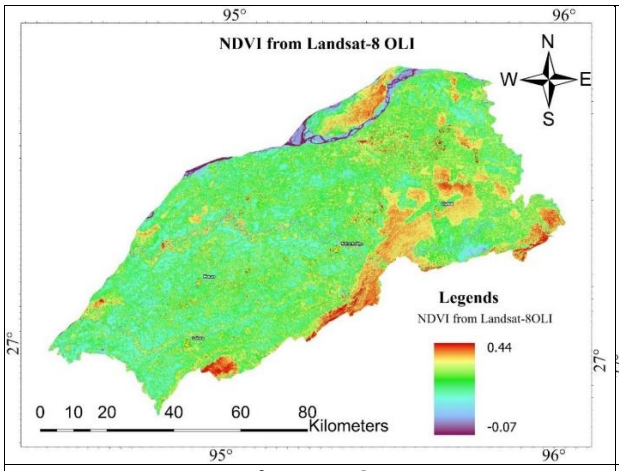

Figure 22- NDVI from Landsat 8-OLI image

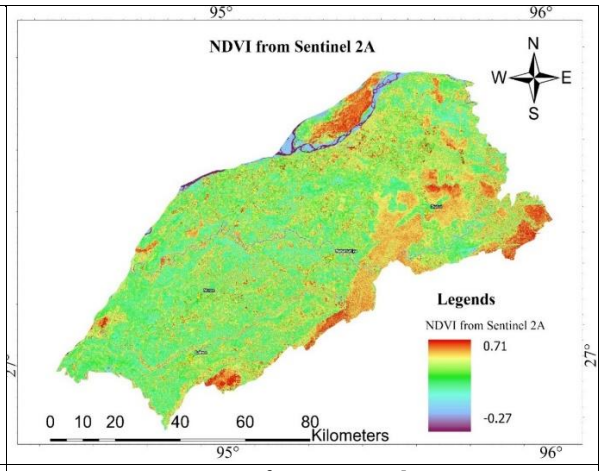

Figure 23- NDVI from Sentinel 2A image

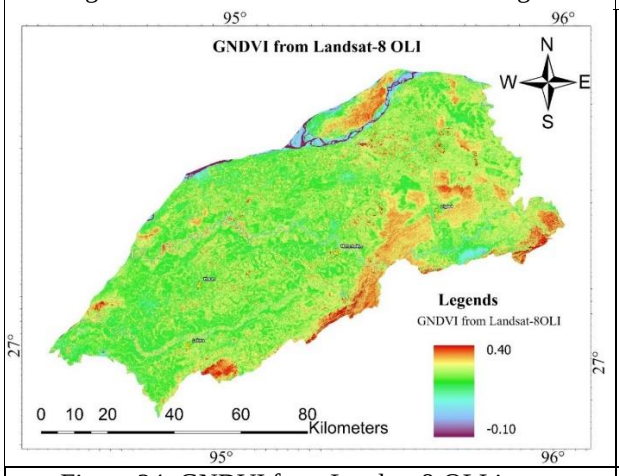

Figure 24- GNDVI from Landsat 8-OLI image

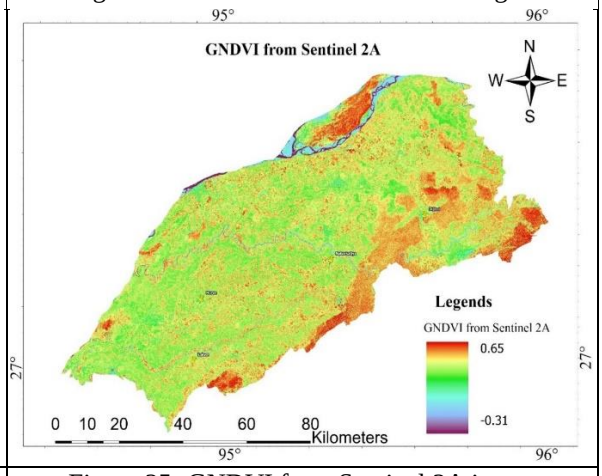

Figure 25- GNDVI from Sentinel 2A image

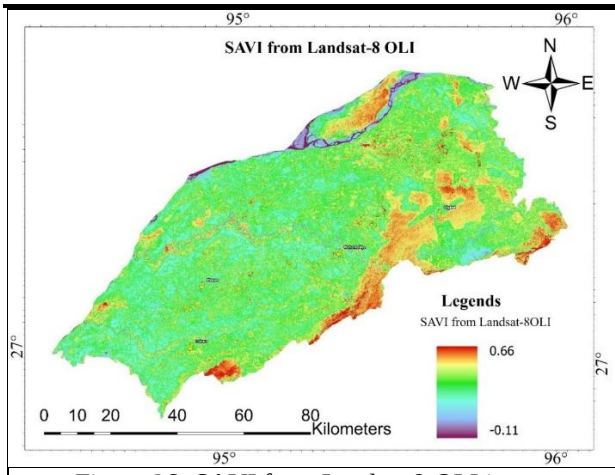

Figure 26- SAVI from Landsat 8-OLI image

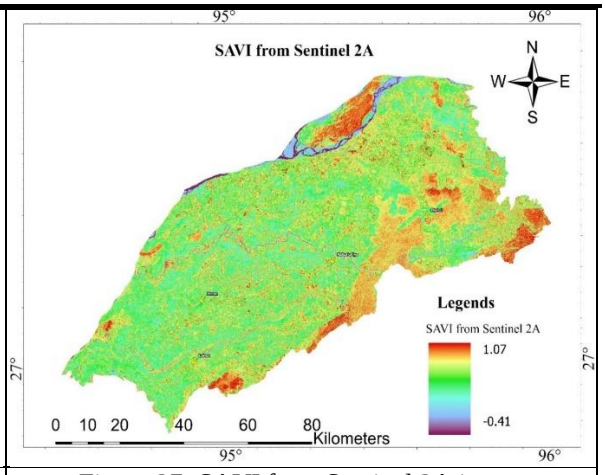

Figure 27- SAVI from Sentinel 2A image

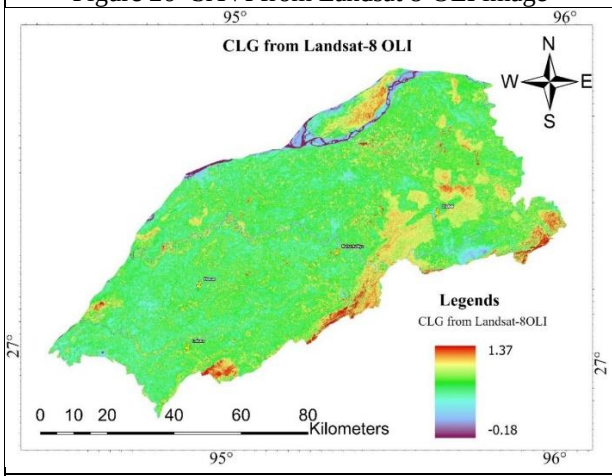

Figure 28- CLG from Landsat 8-OLI image

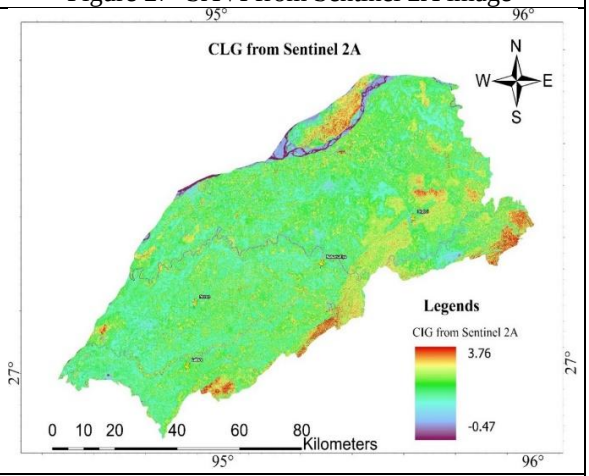

Figure 29- CLG from Sentinel 2A image

Therefore, Vegetation Indices indicated the chemical alteration in the soil and plants present in that area and gave evidence of presence of hydrocarbon micro seepages in Upper Assam Shelf.

5.3 Hydrothermal Alteration

Along with Vegetation Indices and mineral indices, hydrothermal alteration was also performed to cross verify the mineral indices zone in Landsat-8 using ENVI Classic with same band combination for Clay Band6/Band7, (Figure 30), for ferrous Band6/band5 (Figure 31) and for Iron Band 4/band2 (Figure 32)]. It was observed that all hydrothermal alteration images show similar results as obtained from mineral indices.

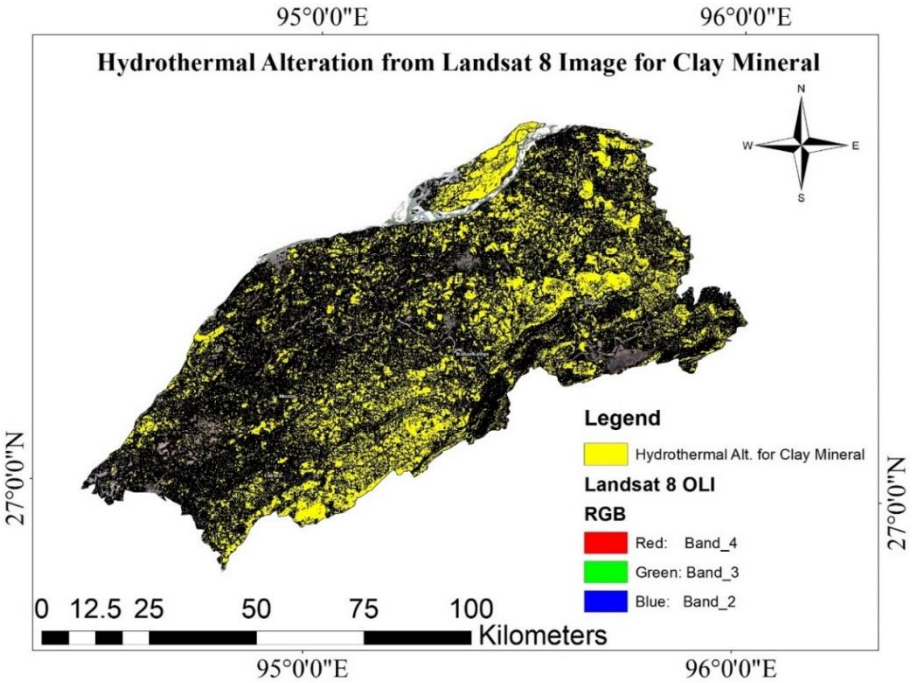

Figure 30- Hydrothermal Alteration zone for Clay Mineral in Landsat 8 image

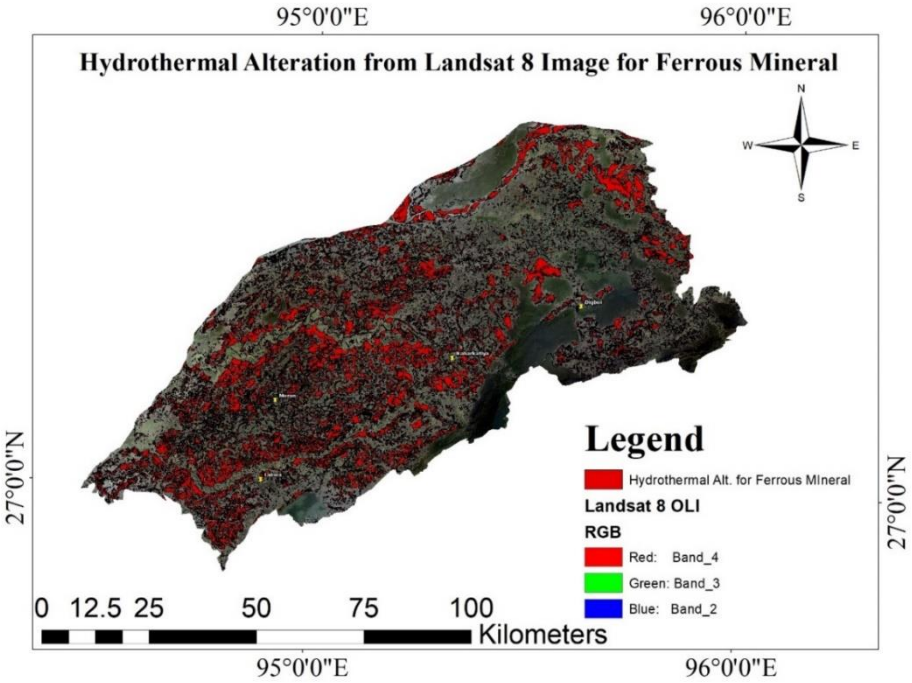

Figure 31- Hydrothermal Alteration zone for ferrous Mineral in Landsat 8 image

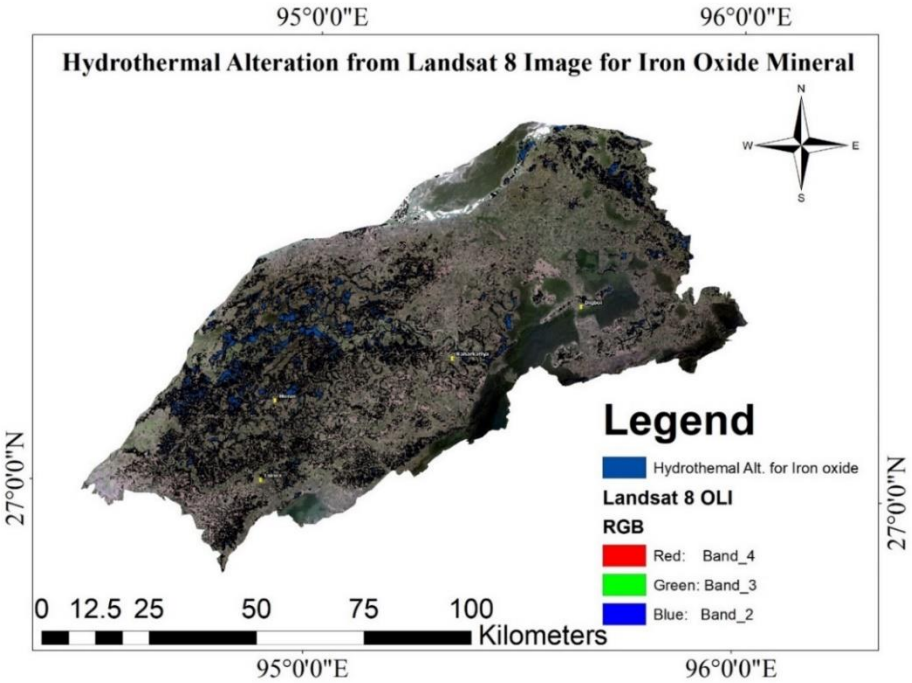

Figure 32- Hydrothermal Alteration zone for Iron Oxide in Landsat 8 image

5.4 Lineaments

Lineament are useful to detect the path of micro seepage through the surface therefore lineaments was extracted form Geomatica and overlapped with Lineaments from Bhukosh, which shows common area of faults and fractures (Figure 33) and was corelated with the mineral indices showing the common zones of mineral alteration and lineaments which indicates that through these faults the hydrocarbon micro seepage might have occurred.

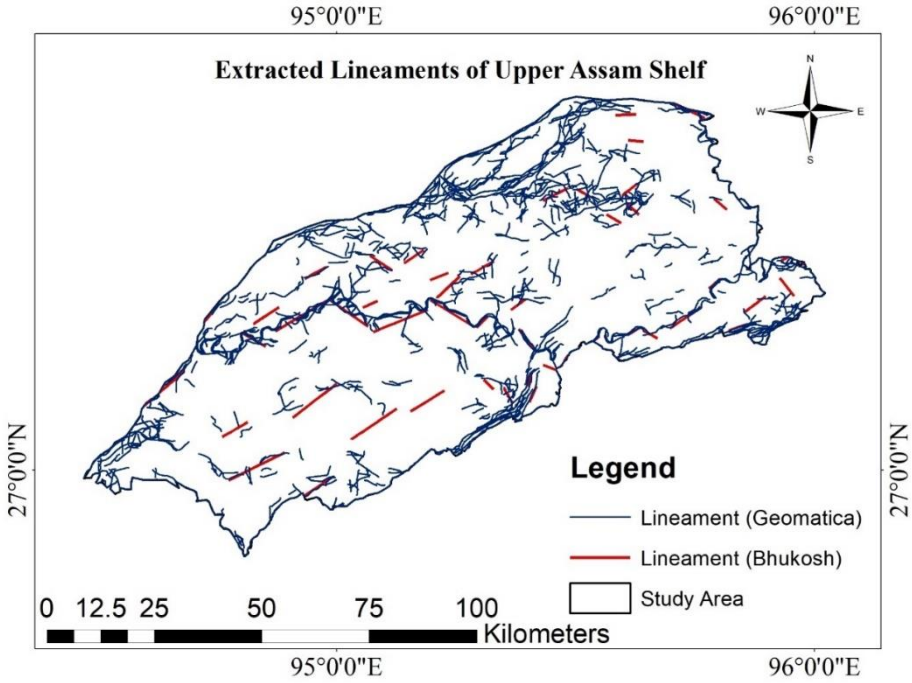

Figure 33- Overlapping of Extracted Lineaments from Geomatica and Bhukosh

The Lineament density map was prepared in Geomatica environment to identify the major faults zones (Figure 34). The red colour area in the image shows highly fractured and fault area which was overlapped with all the

maps and got to know that micro seepages happen through the fault zones (marked in red) (Figure 34) and made mineral alteration and chemical changes in the same zones.

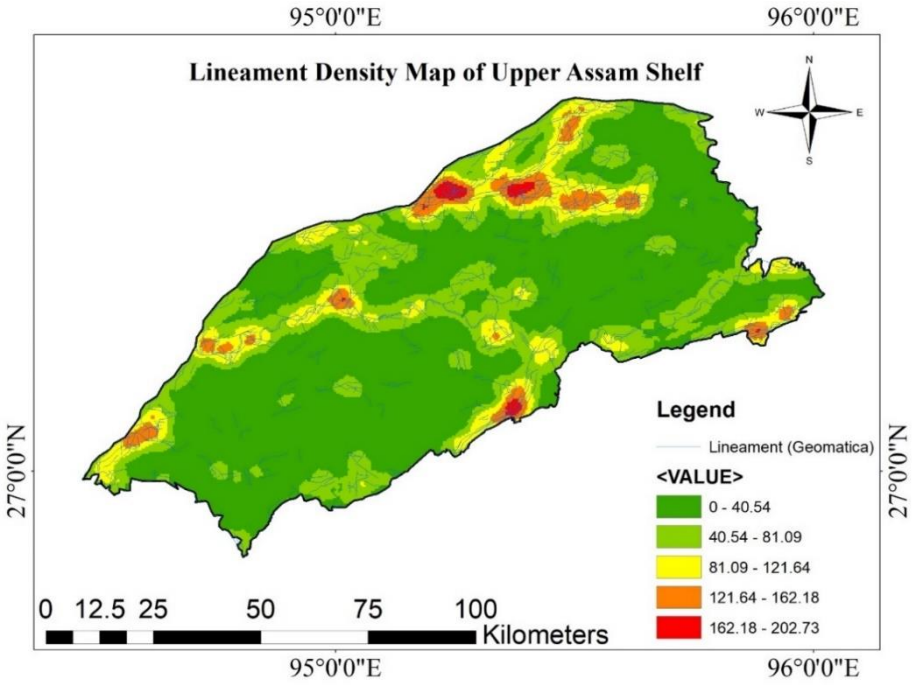

Figure 34- Lineament Density Map

Rose Diagram was prepared using Rockworks, which indicated that major faults and fractures have NE-SW and NNE-SSW direction as seen in (Figure 35).

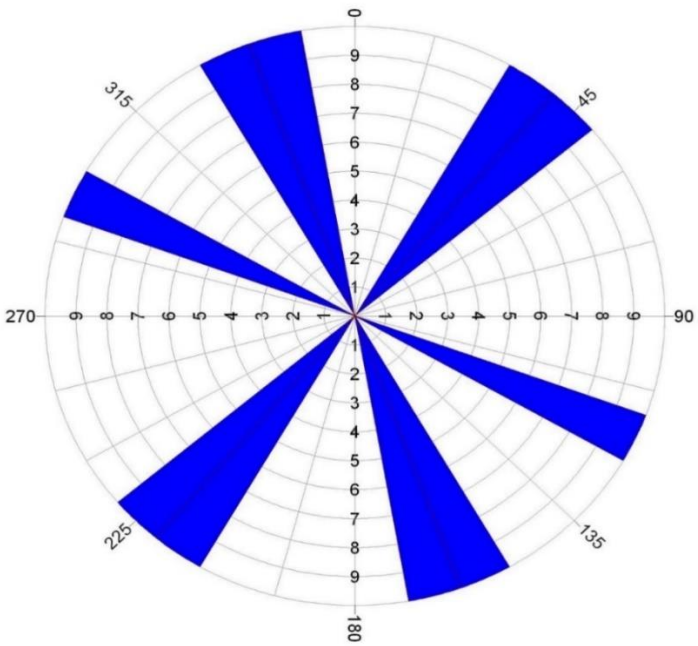

Figure 35- Rose Diagram for Extracted Lineament

Rose Diagram

Statistical Summary	
Calculation Method:	Frequency
Class Interval:	10.0 Degrees
Min.Length Filtering:	Deactivated
Max.Length Filtering:	Deactivated
Azimuth Filtering:	Activated
Minimum Azimuth #1:	0.0 Degrees
Maximum Azimuth #1:	360.0 Degrees
Data Type:	Bidirectional
Population:	5
Total Length of All Lineations:	15,954.03
Maximum Bin Population:	1.0
Mean Bin Population:	1.0
Standard Deviation of Bin Population:	0.0
Maximum Bin Population (%):	10.0
Mean Bin Population (%):	10.0
Standard Deviation of Bin Population (%):	0.0
Maximum Bin Length:	1,701.62
Mean Bin Length:	1,595.4
Standard Deviation of Bin Lengths:	58.24
Maximum Bin Length (%):	10.67
Mean Bin Length (%):	10.0
Standard Deviation of Bin Lengths (%):	0.37
Vector Mean:	179.7 Degrees
	359.7 Degrees
Confidence Interval:	105.4 Degrees
	(80 Percent)
R-mag:	0.22

Figure 36- Rose Diagram values

Therefore, after studying all the data we were able to compare Landsat 8 and Sentinel 2A for better results and vegetation indices shows value of 0.4 for NDVI in Landsat 8 which indicates about the chemical changes, to conform these mineral indices was performed and showed mineral alteration which gave direct evidence for the presence of hydrocarbon. Further, Hydrothermal indices was co-related with mineral indices which resulted into similar result. Gravity data of the study area was very less while magnetic data was high indicating presence of hydrocarbon in the subsurface. Lineament density map shows high fault region for microseepage. Common zones were marked for sparse vegetation, mineral indices, hydrothermal indices, less gravity values, high magnetic values and lineaments resulted into findings of prospective zones of hydrocarbon (Figure 37). Interestingly, the zones which were marked as hydrocarbon prospect lies near the area of major oil fields namely Digboi, Naharkatiya, Moran and Lakwa which can be due to the improper traps.

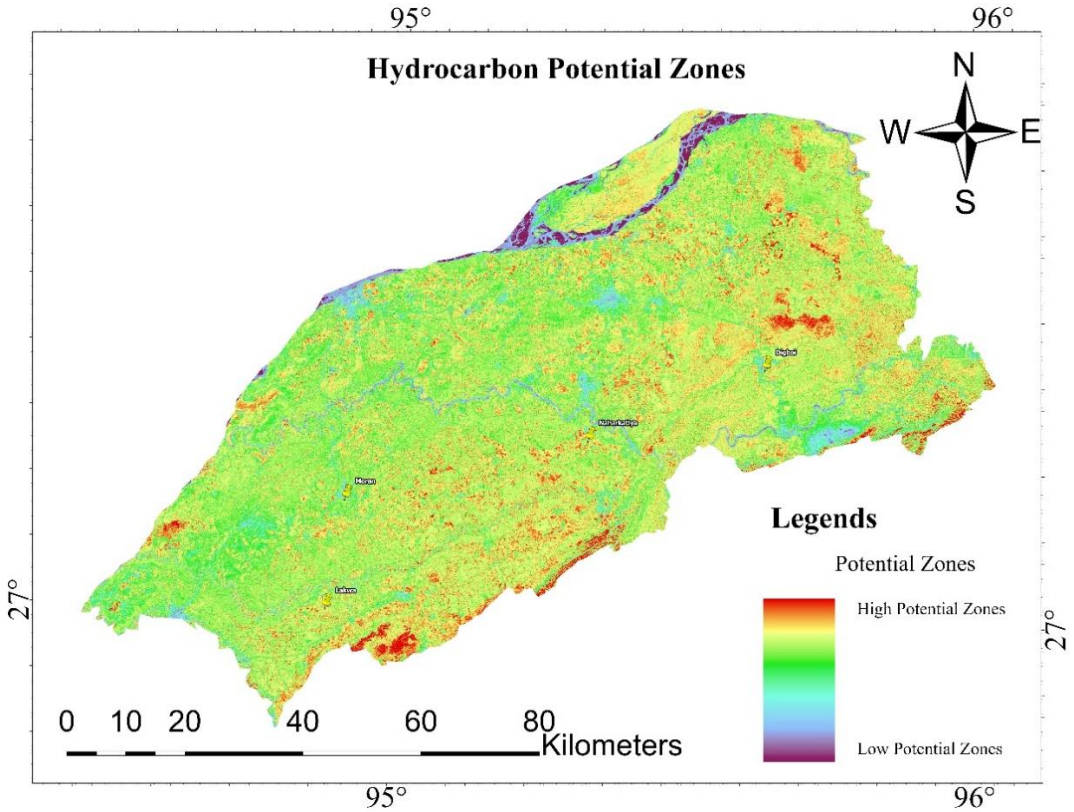

Figure 37- Hydrocarbon Potential Zones

6. Discussion

In order to identify hydrocarbon potential zones in the Upper Assam Shelf region, a combination of remote sensing and spatial analysis techniques were used. Mineral indices such as clay carbonate, ferrous, and iron oxide were used to directly detect the presence of hydrocarbon on the surface, with higher index values indicating mineral alteration and thus the presence of hydrocarbon microseepages. Clay Carbonate Indices showed 1.42 and 2.09 as higher values in red color for Landsat 8 and Sentinel 2, respectively. Ferrous indices showed 2.60 and 3.90 as higher values in red color for Landsat 8 and Sentinel 2, respectively. Iron oxide showed 1.51 and 2.04 as higher values in red color. Higher values in all mineral indices indicate mineral alteration and direct evidence of the presence of hydrocarbons due to microseepages.

Vegetation indices such as NDVI, GNDVI, SAVI, and CLG were used to detect chemical alteration in the soil and vegetation, which provided evidence of possible hydrocarbon microseepages. These indices were found to be effective in detecting sparse vegetation due to chemical alteration, with NDVI values of 0.44 and 0.71. Similarly, GNDVI showed Landsat 8-OLI and Sentinel 2A data, indicating that vegetation indices are a useful tool for identifying potential hydrocarbon zones. Hydrothermal alteration was performed to cross-verify the mineral indices zones, and lineament extraction was used to detect the path of microseepage through the surface. Hydrothermal alteration images showed similar results as the mineral indices. Lineament extraction from Geomatica and Bhukosh showed common areas of faults and fractures, which were correlated with the mineral indices to identify common zones of mineral alteration and lineaments. The density map of the lineaments extracted from Geomatica was used to identify major fault and fracture zones, which were found to have a NE-SW and NNE-SSW direction as shown in the rose diagram prepared using Rockworks2023.

The results showed that the common zones of mineral alteration and lineaments coincided with areas of hydrocarbon prospect, which were located near major oil fields such as Digboi, Naharkatiya, Moran, and Lakwa. This study demonstrates the effectiveness of remote sensing and spatial analysis tools in identifying hydrocarbon potential zones and provides valuable insights for future research in this area. Overall, the combination of vegetation indices, mineral indices, hydrothermal alteration, lineament extraction, and density mapping techniques proved to be an effective way to identify potential hydrocarbon zones in the Upper Assam Shelf region. By correlating the results from these techniques, the study was able to locate common areas of mineral alteration and lineaments that indicated the presence of hydrocarbon microseepages. These findings have important implications for future exploration efforts in the area and highlight the potential of remote sensing and spatial analysis techniques for identifying hydrocarbon potential zones.

7. Conclusion

Based on the findings of this study, it can be concluded that the use of remote sensing techniques is a powerful tool for identifying hydrocarbon prospective zones in a given study area. The use of multispectral images, in combination with geo-structural methods, allowed us to detect anomalies in vegetation that could be attributed to chemical alteration caused by the presence of hydrocarbons. The mineral indices further confirmed the presence of hydrocarbons, and hydrothermal alteration maps were consistent with the mineral indices, providing further evidence of the presence of hydrocarbon micro seepages.

Our analysis of lineaments, which are the surface and subsurface expression of faults, showed that the presence of hydrocarbons on the surface was due to connectivity between the surface and reservoir through faults. By extracting and analyzing lineament densities, we were able to determine the direction of faults from where the micro seepages occurred. The rose diagram we constructed helped us visualize the dominant direction of these faults in the study area.

Thus, using various techniques in remote sensing one can determine the hydrocarbon exporation in the perticular area with the help og mineral indices, vegetation index, hydrothermal alteration, Lineaments and geophysical survey. Overall, the results of this study highlight the importance of integrating remote sensing techniques with geo-structural methods for identifying hydrocarbon prospective zones. This approach provides an efficient, cost-effective, and non-invasive means of identifying potential hydrocarbon reservoirs in a given area, which can be used to guide future exploration and production activities. By locating these zones before exploitation, the risk of

costly exploration efforts with no positive outcome can be minimized, leading to more efficient use of resources and better outcomes for the industry.

References

[1] Adamu, B., Tansey, K., & Ogutu, B. (2015). Using vegetation spectral indices to detect oil pollution in the Niger Delta. Remote Sensing Letters, 6(2), 145–154. https://doi.org/10.1080/2150704X.2015.1015656

[2] Ahmad, W. A., Ahmed, M. A., & Al-Sharia, G. H. (2017). Using Normalized Difference Vegetation Index (NDVI) to Identify Hydrocarbon Seepage in Kifl Oil Field and Adjacent Areas South of Iraq. 7(1). www.iiste.org

[3] Alasta, A. F. (2011). Using Remote Sensing data to identify iron deposits in central western Libya Resolution Enhancement using wavelet Transforms Applied to SODSIM Images View project. https://www.researchgate.net/publication/325550303

[4] Asadzadeh, S., & de Souza Filho, C. R. (2017). Spectral remote sensing for onshore seepage characterization: A critical overview. In Earth-Science Reviews (Vol. 168, pp. 48–72). Elsevier B.V. https://doi.org/10.1016/j.earscirev.2017.03.004

[5] Balogun, A. L., Yekeen, S. T., Pradhan, B., & Althuwaynee, O. F. (2020). Spatio-temporal analysis of oil spill impact and recovery pattern of coastal vegetation and wetland using multispectral satellite Landsat 8-OLI imagery and machine learning models. Remote Sensing, 12(7). https://doi.org/10.3390/rs12071225

[6] Boruah, A., Verma, S., Rasheed, A., Siddharth Gairola, G., & Gogoi, A. (2022). Macro-seepage based potential new hydrocarbon prospects in Assam-Arakan Basin, India. Scientific Reports, 12(1). https://doi.org/10.1038/s41598-022-06045-6

[7] Burazer, M., Grbović, M., & Žitko, V. (2001). Magnetic data processing for hydrocarbon exploration in the Pannonian Basin, Yugoslavia. GEOPHYSICS, 66(6), 1669–1679. https://doi.org/10.1190/1.1486769

[8] Cai, J., Du, J., Song, M., Lei, T., Wang, X., & Li, Y. (2022). Control of clay mineral properties on hydrocarbon generation of organo-clay complexes: Evidence from high-temperature pyrolysis experiments. Applied Clay Science, 216. https://doi.org/10.1016/j.clay.2021.106368

[9] El-Desoky, H. M., Tende, A. W., Abdel-Rahman, A. M., Ene, A., Awad, H. A., Fahmy, W., El-Awny, H., & Zakaly, H. M. H. (2022). Hydrothermal Alteration Mapping Using Landsat 8 and ASTER Data and Geochemical Characteristics of Precambrian Rocks in the Egyptian Shield: A Case Study from Abu Ghalaga, Southeastern Desert, Egypt. Remote Sensing, 14(14). https://doi.org/10.3390/rs14143456

[10] Enoh, M. A., Okeke, F. I., & Okeke, U. C. (2021). Automatic lineaments mapping and extraction in relationship to natural hydrocarbon seepage in Ugwueme, South-Eastern Nigeria. Geodesy and Cartography (Vilnius), 47(1), 34–44. https://doi.org/10.3846/gac.2021.12099

[11] Garain, S., Mitra, D., & Das, P. (2019). Detection of hydrocarbon microseepage-induced anomalies by spectral enhancements of Landsat 7 ETM+ images in part of Assam–Arakan Fold Belt, India. Journal of Petroleum Exploration and Production Technology, 9(4), 2573–2582. https://doi.org/10.1007/s13202-019-00747-w

[12] Garain, S., Mitra, D., & Das, P. (2021). Mapping hydrocarbon microseepage prospect areas by integrated studies of ASTER processing, geochemistry and geophysical surveys in Assam-Arakan Fold Belt, NE India. International Journal of Applied Earth Observation and Geoinformation, 102. https://doi.org/10.1016/j.jag.2021.102432

[13] Gasmi, A., Gomez, C., Chehbouni, A., Dhiba, D., & Elfil, H. (2022). Satellite Multi-Sensor Data Fusion for Soil Clay Mapping Based on the Spectral Index and Spectral Bands Approaches. Remote Sensing, 14(5). https://doi.org/10.3390/rs14051103

[14] Imbroane, A., Melenti, C., & Gorgan, D. (2007). Mineral explorations by landsat image ratios. Proceedings - 9th International Symposium on Symbolic and Numeric Algorithms for Scientific Computing, SYNASC 2007, 335–340. https://doi.org/10.1109/SYNASC.2007.52

[15] Jiang, S. (2012). Clay Minerals from the Perspective of Oil and Gas Exploration. In Clay Minerals in Nature - Their Characterization, Modification and Application. InTech. https://doi.org/10.5772/47790

[16] Kovalev, A., & Tokareva, O. (n.d.). Using MODIS NDVI products for vegetation state monitoring on the oil production territory in Western Siberia. https://doi.org/10.1051/conf

[17] Lammoglia, T., & de Souza Filho, C. R. (2013). Unraveling Hydrocarbon Microseepages in Onshore Basins Using Spectral-Spatial Processing of Advanced Spaceborne Thermal Emission and Reflection Radiometer (ASTER) Data. In Surveys in Geophysics (Vol. 34, Issue 3, pp. 349–373). Kluwer Academic Publishers. https://doi.org/10.1007/s10712-013-9225-3

[18] Mah, A., Taylor, G. R., Lcnnox, P., & Balia, L. (n.d.). AnttcrE Lineament Analysis of Landsat Thematic Mapper lmages, Northern TerritorY, Austtalia.

[19] Mahboob, M. A., Genc, B., Celik, T., Ali, S., & Atif, I. (2019). Mapping hydrothermal minerals using remotely sensed reflectance spectroscopy data from Landsat. Journal of the Southern African Institute of Mining and Metallurgy, 119(3), 279–289. https://doi.org/10.17159/2411-9717/2019/v119n3a7

[20] Noomen, M. F., van der Werff, H. M. A., & van der Meer, F. D. (2012). Spectral and spatial indicators of botanical changes caused by long-term hydrocarbon seepage. Ecological Informatics, 8, 55–64. https://doi.org/10.1016/j.ecoinf.2012.01.001

[21] Pour, A. B., & Hashim, M. (2015). Hydrothermal alteration mapping from Landsat-8 data, Sar Cheshmeh copper mining district, south-eastern Islamic Republic of Iran. Journal of Taibah University for Science, 9(2), 155–166. https://doi.org/10.1016/j.jtusci.2014.11.008

[22] Prabaharan, S., Ramalingam, M., Subramani, T., & Lakshumanan, C. (2013). Remote Sensing and GIS Tool to Detect Hydrocarbon Prospect in Nagapattinam Sub Basin, India. Geotechnical and Geological Engineering, 31(1), 267–277. https://doi.org/10.1007/s10706-012-9589-z

[23] Putra, M. I. J., Huda, D. N., Afdhalia, F., & Supriatna. (2019). Onshore oil and gas reservoir detection through mapping of hydrocarbon microseepage using remote sensing. IOP Conference Series: Earth and Environmental Science, 311(1). https://doi.org/10.1088/1755-1315/311/1/012083

[24] Schumacher, D. (n.d.). Surface Geochemical Exploration for Petroleum.

[25] Wu, L. M., Zhou, C. H., Keeling, J., Tong, D. S., & Yu, W. H. (2012). Towards an understanding of the role of clay minerals in crude oil formation, migration and accumulation. In Earth-Science Reviews (Vol. 115, Issue 4, pp. 373–386). https://doi.org/10.1016/j.earscirev.2012.10.001